

Accepted Manuscript

A dual chemosensor for Cu^{2+} and Fe^{3+} based on π -extend tetrathiafulvalene derivative

Yuwen Ma, Taohua Leng, Yarong Qu, Chengyun Wang, Yongjia Shen, Weihong Zhu



PII: S0040-4020(16)31188-7

DOI: [10.1016/j.tet.2016.11.033](https://doi.org/10.1016/j.tet.2016.11.033)

Reference: TET 28247

To appear in: *Tetrahedron*

Received Date: 29 September 2016

Revised Date: 8 November 2016

Accepted Date: 14 November 2016

Please cite this article as: Ma Y, Leng T, Qu Y, Wang C, Shen Y, Zhu W, A dual chemosensor for Cu^{2+} and Fe^{3+} based on π -extend tetrathiafulvalene derivative, *Tetrahedron* (2016), doi: 10.1016/j.tet.2016.11.033.

This is a PDF file of an unedited manuscript that has been accepted for publication. As a service to our customers we are providing this early version of the manuscript. The manuscript will undergo copyediting, typesetting, and review of the resulting proof before it is published in its final form. Please note that during the production process errors may be discovered which could affect the content, and all legal disclaimers that apply to the journal pertain.

Graphical Abstract

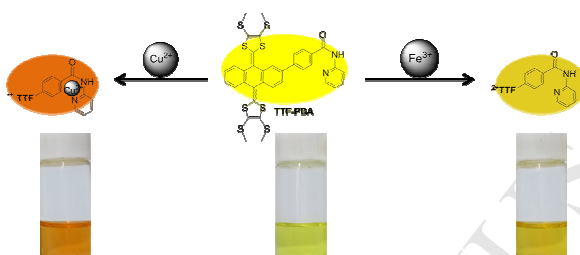
A dual chemosensor for Cu^{2+} and Fe^{3+} based on π -extend tetrathiafulvalene derivative

Yuwen Ma^a, Taohua Leng^b, Yarong Qu^a, Chengyun Wang^{a,*}, Yongjia Shen^a, Weihong Zhu^{a,*}

^a Key Laboratory for Advanced Materials and Institute of Fine Chemicals, East China University of Science & Technology, Shanghai 200237, P. R. China.

^b National Food Quality Supervision and Inspection Center (Shanghai) / Shanghai Institute of Quality Inspection and Technical Research, Shanghai 200233, P. R. China.

An exTTF-based dual chemosensor for selective and sensitive detection of copper (II) and iron (III) in different signal pathways was prepared. Furthermore, when Fe^{3+} existed, Cu^{2+} can be detected sequentially by the sensor.





Tetrahedron

journal homepage: www.elsevier.com



A dual chemosensor for Cu²⁺ and Fe³⁺ based on π -extend tetrathiafulvalene derivative

Yuwen Ma^a, Taohua leng^b, Yarong Qu^a, Chengyun Wang^{a*}, Yongjia Shen^a, Weihong Zhu^{a*}

^a Key Laboratory for Advanced Materials and Institute of Fine Chemicals, East China University of Science & Technology, Shanghai 200237, P. R. China.

^b National Food Quality Supervision and Inspection Center (Shanghai) / Shanghai Institute of Quality Inspection and Technical Research, Shanghai 200233, P. R. China.

ARTICLE INFO

Article history:

Received

Received in revised form

Accepted

Available online

Keywords:

 π -extend tetrathiafulvalene,

dual chemosensor,

copper (II),

iron (III)

ABSTRACT

A new dual chemosensor (**TTF-PBA**) for Fe³⁺ and Cu²⁺ in different signal pathways was designed and synthesized. The absorption spectrum, fluorescence spectrum and cyclic voltammograms changed in the presence of Cu²⁺ and Fe³⁺. The optical color changed within 5 seconds from yellow to orange upon the addition of Cu²⁺, and it changed to dark yellow when Fe³⁺ existed. The cyclic voltammogram of Cu²⁺/TTF-PBA changed from E_{ox}=0.50V, E_{red}=0.32V to E_{ox}=0.64V, E_{red}=0.80V (vs Ag/AgCl) upon the addition of 2.0 equiv. Cu²⁺. As for Fe³⁺/TTF-PBA, its oxidation wave disappeared, and its reduction wave appeared at E_{red}=-0.59V (vs Ag/AgCl) upon the addition of 4.0 equiv. Fe³⁺. The sensor displayed high selectivity for Cu²⁺ and Fe³⁺ over other ions including Pb²⁺, Zn²⁺, Ni²⁺, Ag⁺, Cr³⁺, Mn²⁺, Al³⁺, Co²⁺, Pd²⁺, Hg²⁺, Fe²⁺, Cd²⁺, Ce³⁺, Bi³⁺ and Au³⁺, the detection limits for Cu²⁺ and Fe³⁺ ion reached as low as 5.33×10⁻⁷ mol/L and 5.34×10⁻⁷ mol/L, respectively. Furthermore, when Fe³⁺ existed, Cu²⁺ can be detected sequentially by the sensor through the absorption spectrum and the color change observed by naked-eyes.

2015 Elsevier Ltd. All rights reserved.

1. Introduction

Recently, much attention has been paid to the design of chemosensors for the selective detection of heavy metal ions due to their potential applications in many fields including chemistry, biology, medicine and environment¹⁻³. Iron (Fe³⁺) is one of the most essential trace elements, it performs a major function in the cells of all organisms systems and in various cellular biochemical processes⁴. The iron deficiency can cause anemia, hemochromatosis, liver damage, diabetes, Parkinson's disease and cancer etc.⁵. Nonetheless, iron excess in the blood and cells can lead to an increased generation of reactive oxygen species via Fenton chemistry, which causes undesirable reactions with biomolecules contributing to induce cell death⁶. Copper (Cu²⁺), another heavy metal ion, is utilized as a catalytic co-factor for various metalloenzymes, including superoxide dismutase, cytochrome c oxidase, tyrosinase and nuclease^{7,8}. However, excessive copper in cellular can cause serious neurodegenerative diseases, such as Alzheimer's, Menkes and Wilson's diseases⁹. It may also cause infant liver damage^{10,11} and childhood cirrhosis¹² when copper is accumulated excessively in the body. Due to the above special properties of Fe³⁺ and Cu²⁺, it is very necessary to develop methods for the detection of these two metal ions. Although various colorimetric and fluorescent sensors for Fe³⁺ or

Cu²⁺ were investigated, only a few of them can be used for detection of both Fe³⁺ and Cu²⁺ in different signal pathways¹³⁻¹⁶.

Tetrathiafulvalene (TTF) and its derivatives play a leading role in making redox sensors for metal ions based on its electron-donating and electrochemical properties¹⁷. Usually, TTF possesses a remarkable π -electron donor property and can result in two sequential and reversible oxidation processes to generate cation radical (TTF^{•+}) and dication (TTF²⁺) species. In particular, TTF containing *p*-quinodimethane analogues (named π -extend TTF) can be oxidized at lower potential due to its charge delocalization and a decreased Coulombic repulsion in the dicationic state¹⁸⁻²⁰. Based on these particular electronic and geometrical features, the TTF containing *p*-quinodimethane framework was used as redox-active sensor in previous experiments²¹.

As reported before, two optical chemosensors were designed by our group based on π -extend TTF, with di(pyridine-2-ylmethyl)amine used as receptor. These two dyes show high sensitivity and selectivity just for Cu²⁺²². In this work, we have designed and synthesized a new dual chemosensor based on 2,2'-(2-iodoanthracene-9,10-diylidene)bis(4,5-bis(methylthio)-1,3-dithiole) (π -extend TTF), which can be used for detecting both Fe³⁺ and Cu²⁺ in different signal pathways. In the new chemosensor, π -extend TTF is used as electron donor and picolinamide unit is used as electron acceptor. It is anticipated

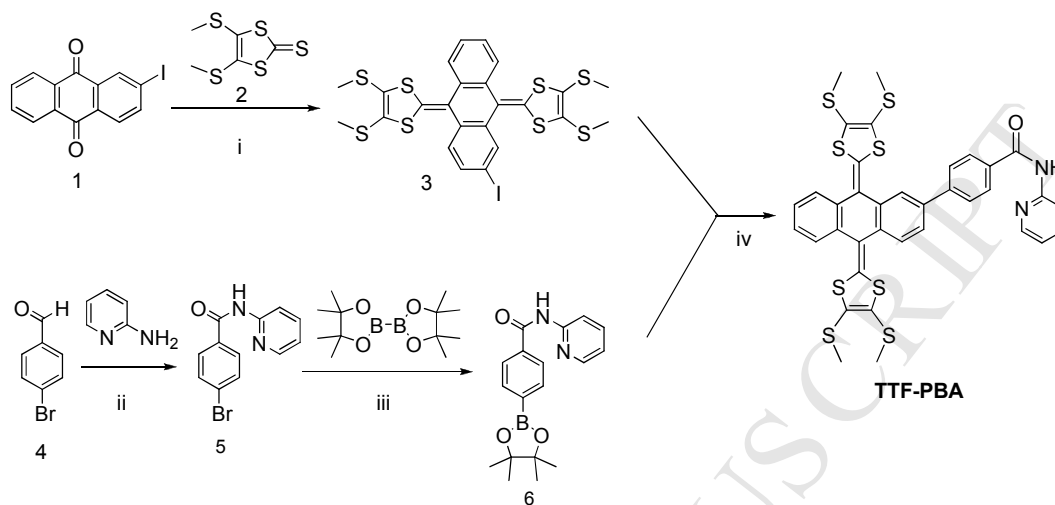
* Corresponding author: Tel/fax: +086-21-64252967; E-mail address: cywang@ecust.edu.cn (C. -Y. Wang), whzhu@ecust.edu.cn (W.-H. Zhu)

that the chemosensor can exhibit high sensitivity and selectivity for Fe^{3+} and Cu^{2+} .

TTF-PBA (The synthetic route shown in **Scheme 1**) was synthesized in four steps and was easy to modify. The last step was processed by Suzuki coupling reaction in 49.6% yield. The chemical structure of TTF-PBA was confirmed by $^1\text{H-NMR}$, $^{13}\text{C-NMR}$ and mass spectroscopic data. (**Fig.S1 - S6**)

2. Results and discussion

2.1 Synthesis



i) $\text{P}(\text{OEt})_3/\text{toluene}$, 100°C , overnight, 52.51%. (ii) DMF/CuI , 80°C , 24h, 62.79%. (iii) dioxane/ $\text{KOAc}/\text{Pd}(\text{dppf})\text{Cl}_2$, 100°C , overnight, 72.03%. (iv) toluene/ $\text{H}_2\text{O}/\text{K}_2\text{CO}_3/\text{Pd}(\text{PPh}_3)_4$, reflux, 24h, 49.62%.

Scheme 1 The synthetic route of TTF-PBA.

2.2. The sensing responses for Cu^{2+} with TTF-PBA

To evaluate the sensing behavior of the dye TTF-PBA towards Cu^{2+} , the absorption spectral titration of TTF-PBA with Cu^{2+} in acetonitrile was carried out.

As shown in **Fig.1(a)**, two absorption bands of TTF-PBA were centered at 375 nm and 439 nm in acetonitrile. Upon addition of Cu^{2+} into the solution, the absorption band at 439 nm disappeared gradually. When the amount of Cu^{2+} achieved at 2.0 equiv., two new bands appeared at 417 nm, 467 nm and the band at 375 nm blue-shifted to 362 nm gradually. Through the detection of Job's Plot, the band at 467 nm experienced dramatically increased and then decreased process. The phenomenon can infer that picolinamide unit of the dye acts as a ligand in complex with Cu^{2+} ion to form a four membered ring²³, in which, the two nitrogen atoms participate in coordination. Furthermore, the ratio between Cu^{2+} and TTF-PBA was confirmed by the Job's Plot (**Fig.2**). The change of Job's Plot happened at $[\text{Cu}^{2+}]/([\text{Cu}^{2+}]+[\text{TTF-PBA}])=0.5$, which meant that

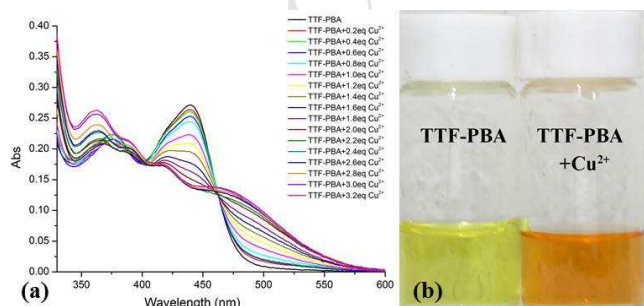


Fig. 1 (a) UV-vis spectra of TTF-PBA in acetonitrile (2×10^{-5} mol/L) upon addition of 0.2-3.2 equiv. CuCl_2 . (b) Color change of the addition of 3.0 equiv. of CuCl_2 into TTF-PBA solution (1×10^{-4} mol/L).

Cu^{2+} and TTF-PBA formed a complex with a ratio of 1:1. The binding constant (K_a) was estimated using Benesi-Hildebrand

plot, which was done by absorbance changes of consequent titration ($1/(A-A_0)$) against $1/[\text{Cu}^{2+}]$, where A_0 is the absorbance of free TTF-PBA, A is the absorbance of TTF-PBA with Cu^{2+} in different concentration (**Fig.S7**). The magnitude of K_a was calculated from the ratio of intercept/slope of the straight line, and estimated value is about 1.32×10^4 L/mol. With the addition of more Cu^{2+} into the solution, the two new bands at 461 nm and 419 nm were almost not changed, while a new small one appeared at 389 nm (**Fig.1(a)**). This phenomenon may be caused by the oxidizing effect between Cu^{2+} and TTF-PBA. The spectrum did not show any change until the Cu^{2+} amount achieved at 3.0 equiv. The solution color began to change from light yellow to light orange with the addition of 2.0 equiv. Cu^{2+} , and with the more amount of Cu^{2+} , the color changed to orange. All the color changes happened within 5 seconds. When the amount of Cu^{2+} reached at 3.0 equiv., the color did not change any more.

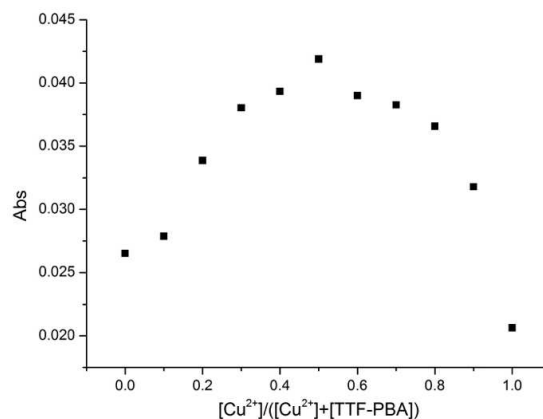


Fig. 2 Job's Plot for the complex of Cu^{2+} with TTF-PBA determined by UV-vis spectra.

The fluorescence titration studies of TTF-PBA for Cu^{2+} were also carried out. The assessment of the selectivity of TTF-PBA towards Cu^{2+} was studied by fluorescence spectroscopy, which was given in Fig.3.

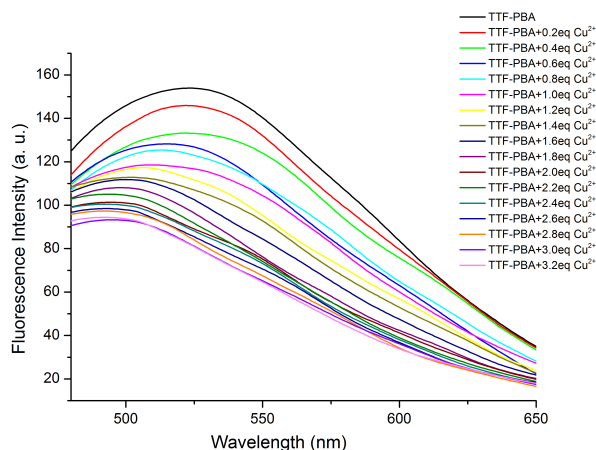


Fig. 3 Fluorescence emission spectra of TTF-PBA (2×10^{-5} mol/L) in acetonitrile upon addition of 0.2-3.2 equiv. of CuCl_2 .

As shown in Fig.3, the fluorescence emission wavelength of TTF-PBA appeared at 522 nm when excited by 430 nm photon. Then the fluorescence quenched gradually with the addition of Cu^{2+} into the solution, and the fluorescence quenched mostly till the Cu^{2+} amount achieved at 3.0 equiv., and the emission wavelength blue-shifted to 496 nm. The ratio of the final fluorescence intensity to the initial fluorescence intensity was found to be 0.59. The quenching property of Cu^{2+} can be attributed to its paramagnetic nature with unfilled d-shell^{24, 25}. The detection limit was calculated to be 5.33×10^{-7} M using $3\sigma/K$ (Fig.S8).

2.3 Electrochemical sensing properties of TTF-PBA for Cu^{2+}

Electrochemical sensing for Cu^{2+} by the dye TTF-PBA was also investigated. The electrochemical property of TTF-PBA was carried out on CHI620e electrochemistry workstation in acetonitrile solution. As shown in Fig.4, TTF-PBA underwent an oxidation wave at $E_{\text{ox}}=0.50\text{V}$ (vs Ag/AgCl) and a reduction wave at $E_{\text{red}}=0.32\text{V}$ (vs Ag/AgCl) for that TTF containing anthraquinone exhibited a two-electron redox wave²⁶. This meant that TTF-PBA underwent a reversible redox process.

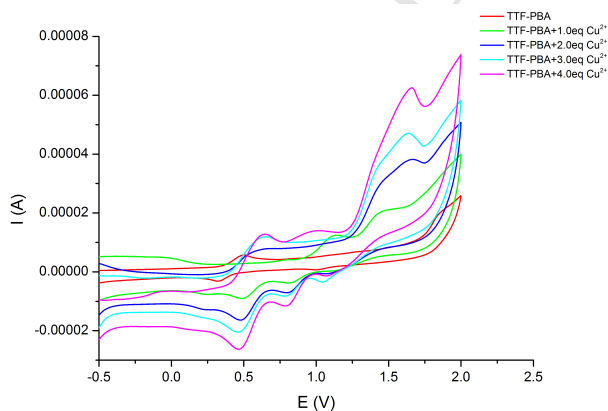


Fig. 4 Cyclic voltammogram of TTF-PBA (1×10^{-3} mol/L) upon addition of 0-4.0 equiv. CuCl_2 (vs Ag/AgCl).

Upon gradual addition of Cu^{2+} into TTF-PBA solution, the oxidation wave and reduction wave were changed (Fig.4). Upon addition of 1.0 equiv. Cu^{2+} , the oxidation wave of TTF-PBA

shifted from $E_{\text{ox}}=0.50\text{V}$ to $E_{\text{ox}}=1.12\text{V}$ (vs Ag/AgCl), and the reduction wave shifted from $E_{\text{red}}=0.32\text{V}$ to $E_{\text{red}}=0.50\text{V}$ (vs Ag/AgCl). These changes can be explained by the formation of complex between Cu^{2+} and TTF-PBA²⁷, which was proved by the Job's Plot. When 2.0 equiv. Cu^{2+} was added into the solution, a new oxidation wave appeared at $E_{\text{ox}}=0.64\text{V}$ (vs Ag/AgCl) and a new reduction wave at $E_{\text{red}}=0.80\text{V}$ (vs Ag/AgCl) appeared gradually upon addition of Cu^{2+} . With the addition of 4.0 equiv. Cu^{2+} into the solution, the waves became much clearly. These phenomena may be caused by the oxidation of TTF unit to cation radical ($\text{TTF}^{\cdot+}$). From the cyclic voltammograms, the new oxidation and reduction waves may arise from the appearance of cation radical TTF-PBA.

2.4. The sensing responses for Fe^{3+} with TTF-PBA

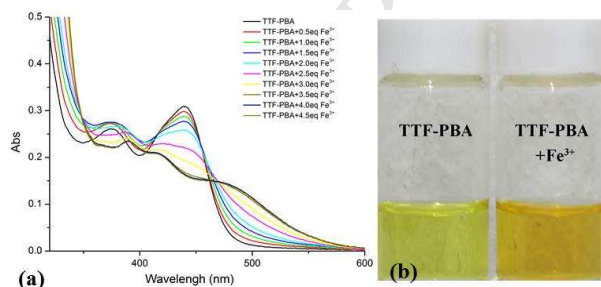


Fig. 5 (a) UV-vis spectra of TTF-PBA in acetonitrile (2×10^{-5} mol/L) upon addition of 0.5-4.5 equiv. FeCl_3 , (b) Color change of the addition of 4.0 equiv. of FeCl_3 into TTF-PBA solution (1×10^{-4} mol/L).

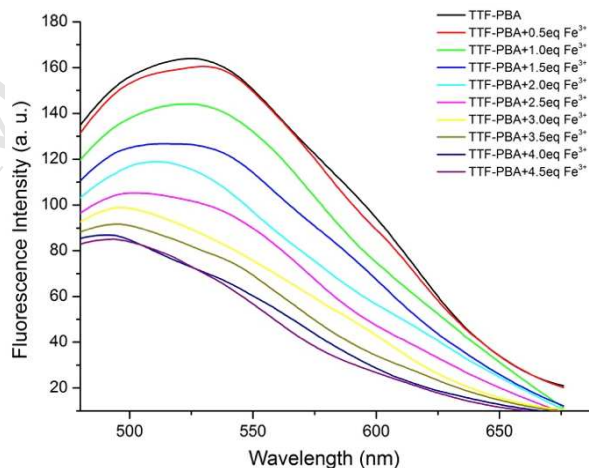


Fig. 6 Fluorescence emission spectra of TTF-PBA (2×10^{-5} mol/L) in acetonitrile upon addition of 0.5-4.5 equiv. of FeCl_3 .

With further study, we found that the dye TTF-PBA can be also used as chemosensor for detecting Fe^{3+} in acetonitrile. To study the sensing property, the absorption titration of TTF-PBA for Fe^{3+} was carried out. Unlike addition of Cu^{2+} , with the increasing of Fe^{3+} , three new small bands appeared at 389 nm, 416 nm and 482 nm, and the two characteristic bands of TTF-PBA at 375 nm and 439 nm were disappeared almost at the same time (Fig.5(a)). These phenomena may result from the oxidation of TTF unit to dication in the dye by Fe^{3+} , for such π -extend TTF can be oxidized at lower potential due to charge delocalization and a decreased Coulombic repulsion in the dication state²⁸. The different absorption spectra of TTF-PBA/ Cu^{2+} and TTF-PBA/ Fe^{3+} indicated that the TTF-PBA exhibited a high selectivity for Cu^{2+} and Fe^{3+} with a different color change. As shown in Fig.5(b), the solution color began to change upon additional of 3.0 equiv. Fe^{3+} , and the solution color changed from light yellow to dark yellow when 4.0 equiv. Fe^{3+} existed. The color did not change when more Fe^{3+} was added. All the color changes happened within 5 seconds.

As shown in fluorescence spectroscopy, Fe^{3+} quenched the fluorescence (excited by 430 nm photon) with a little change in the shape of the spectra as the same as the influence of Cu^{2+} , which was shown in **Fig.6**. The ratio of the final fluorescence intensity to the initial fluorescence intensity was 0.59. As reported, the fluorescence of oxidized TTF was increased²⁹, but the fluorescence of the TTF-PBA solution with Fe^{3+} existed was quenched. It may be attributed to that Fe^{3+} possesses the same paramagnetic nature of Cu^{2+} , and the paramagnetic nature plays a leading role, as a result, the fluorescence is quenched. The detection limit was calculated as 5.34×10^{-7} M using $3\sigma/K$ (**Fig.S9**).

2.5 Electrochemical sensing properties of TTF-PBA for Fe^{3+}

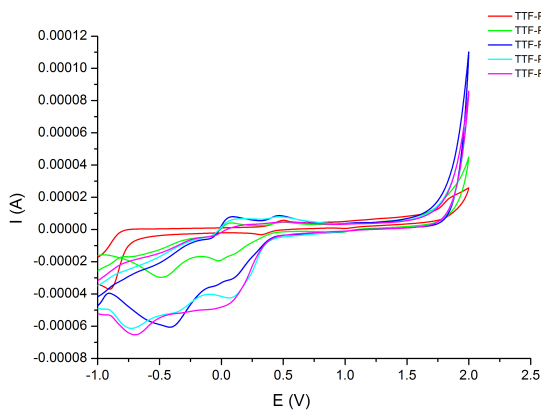


Fig. 7 Cyclic voltammogram of TTF-PBA (1×10^{-3} mol/L) upon addition of 0-4.0 equiv. FeCl_3 (vs Ag/AgCl).

The cyclic voltammogram of TTF-PBA with Fe^{3+} was different from that of Cu^{2+} (**Fig.7**). With the addition of 1.0 equiv. Fe^{3+} , the oxidation wave shifted from $E_{\text{ox}} = -0.50$ V to $E_{\text{ox}} = -0.06$ V (vs Ag/AgCl) and reduction wave shifted from $E_{\text{red}} = -0.32$ V to $E_{\text{red}} = -0.48$ V (vs Ag/AgCl). With the amount of Fe^{3+} increased, the oxidation wave at 0.06 V and the reduction wave at -0.48 V disappeared and a new one appeared at $E_{\text{red}} = -0.59$ V (vs Ag/AgCl). With the addition of 4.0 equiv. Fe^{3+} into the solution, the waves did not change. From the change of cyclic voltammogram, it can be inferred that the TTF unit of TTF-PBA is oxidized to dication species (TTF^{2+}) by Fe^{3+} , as a result, the oxidation wave is disappeared. The dication species (TTF^{2+}) changes to fully aromatic unit, and may conjugate with the picolinamide unit, therefore, the structure is not easy to be restored²⁸.

2.6 The selectivity detection study for Cu^{2+} and Fe^{3+} with TTF-PBA

High selectivity is one of the basic requirements for the chemosensor to successfully recognize the target from various metal ions. The ability of TTF-PBA recognizing Cu^{2+} or Fe^{3+} was evaluated in acetonitrile by observing the changes in the absorption spectra (**Fig.8(a)**). It showed no drastic absorbance change with the additional metal ions (Pb^{2+} , Zn^{2+} , Ni^{2+} , Ag^+ , Cr^{3+} , Mn^{2+} , Al^{3+} , Co^{2+} , Pd^{2+} , Hg^{2+} , Fe^{2+} , Cd^{2+} , Ce^{3+} , Bi^{3+} and Au^{3+}) in the solution. Therefore, the solution color only changed by Cu^{2+} and Fe^{3+} . (**Fig.8(b)**)

To estimate the selectivity of TTF-PBA by fluorescence intensity, other metal ions (Pb^{2+} , Zn^{2+} , Ni^{2+} , Ag^+ , Cr^{3+} , Mn^{2+} , Al^{3+} , Co^{2+} , Pd^{2+} , Hg^{2+} , Fe^{2+} , Cd^{2+} , Ce^{3+} , Bi^{3+} and Au^{3+}) were used for the fluorescence studies in acetonitrile. The changes of fluorescence emission intensity of TTF-PBA in the presence of

different ions were shown in **Fig.9**. It was found that upon addition of various metal ions, the solution exhibited little change in fluorescence intensity. However, Cu^{2+} and Fe^{3+} induced the most pronounced fluorescence quenching respectively. According to Stern-Volmer quenching constants (K_{SV}) in **Table 1**, the constants of TTF-PBA/ Cu^{2+} and TTF-PBA/ Fe^{3+} are larger than that of other ions, which means that TTF-PBA is easier to combine with Cu^{2+} or Fe^{3+} . Therefore, the results showed that TTF-PBA possessed an excellent selectivity for Cu^{2+} and Fe^{3+} ions in fluorescence changes.

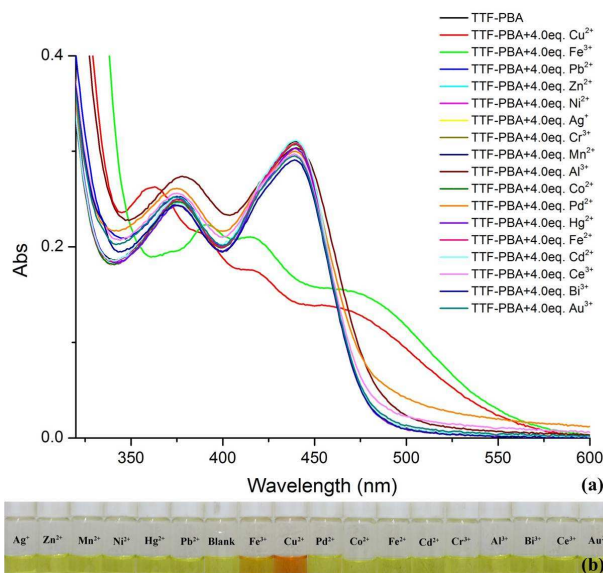


Fig. 8 (a) UV-vis spectra of TTF-PBA in acetonitrile (2×10^{-5} mol/L) upon addition of CuCl_2 , FeCl_3 , AgNO_3 , ZnCl_2 , MnCl_2 , NiCl_2 , $\text{Hg}(\text{COOH})_2$, PbCl_2 , PdCl_2 , CoCl_2 , FeCl_2 , CdCl_2 , CrCl_3 , AlCl_3 , $\text{Ce}_2(\text{SO}_4)_3$, BiCl_3 , AuCl_3 . (**b**) Color changes of TTF-PBA solution (1×10^{-4} mol/L) in presence of different metal ions (4.0 equiv.).

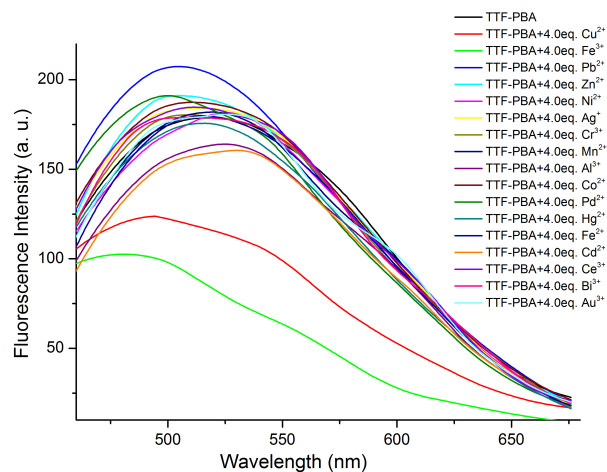


Fig. 9 Fluorescence emission spectra of TTF-PBA in acetonitrile (2×10^{-5} mol/L) upon addition of CuCl_2 , FeCl_3 , AgNO_3 , ZnCl_2 , MnCl_2 , NiCl_2 , $\text{Hg}(\text{COOH})_2$, PbCl_2 , PdCl_2 , CoCl_2 , FeCl_2 , CdCl_2 , CrCl_3 , AlCl_3 , $\text{Ce}_2(\text{SO}_4)_3$, BiCl_3 , AuCl_3 .

Furthermore, as shown in **Fig.10**, when other ions such as Pb^{2+} , Zn^{2+} , Ni^{2+} , Ag^+ , Cr^{3+} , Mn^{2+} , Al^{3+} , Co^{2+} , Pd^{2+} , Hg^{2+} , Fe^{2+} , Cd^{2+} , Ce^{3+} , Bi^{3+} and Au^{3+} existed in the solution of TTF-PBA, Cu^{2+} and Fe^{3+} quenched the fluorescence respectively, illustrating that other ions did not interfere with the detection of Cu^{2+} and Fe^{3+} , which meant that TTF-PBA exhibited high selectivity for Cu^{2+} and Fe^{3+} over other metal ions.

Table 1 The Stern-Volmer quenching constants (K_{SV})

Ions	Pb ²⁺	Zn ²⁺	Ni ²⁺	Ag ⁺	Cr ³⁺	Mn ²⁺	Al ³⁺	Co ²⁺	Cd ²⁺
K _{SV}	380.3	1309.6	1811.8	1621.4	1979.5	1758.7	3317.9	1432.4	3734.4
Ions	Pd ²⁺	Hg ²⁺	Fe ²⁺	Ce ³⁺	Bi ³⁺	Au ³⁺	Cu ²⁺	Fe ³⁺	
K _{SV}	1766.6	2326.6	1998.9	2024.8	1841.9	2107.7	8686.4	8686.4	

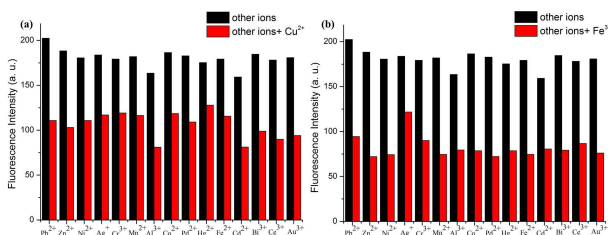


Fig. 10 (a) The selectivity of TTF-PBA in acetonitrile (2×10^{-5} mol/L) for Cu²⁺ in the presence of other metal ions (Pb²⁺, Zn²⁺, Ni²⁺, Ag⁺, Cr³⁺, Mn²⁺, Al³⁺, Co²⁺, Pd²⁺, Hg²⁺, Fe²⁺, Cd²⁺, Ce³⁺, Bi³⁺, Au³⁺) (wavelength: 522 nm). (b) The selectivity of TTF-PBA in acetonitrile (2×10^{-5} mol/L) for Fe³⁺ in the presence of other metal ions (Pb²⁺, Zn²⁺, Ni²⁺, Ag⁺, Cr³⁺, Mn²⁺, Al³⁺, Co²⁺, Pd²⁺, Hg²⁺, Fe²⁺, Cd²⁺, Ce³⁺, Bi³⁺, Au³⁺) (wavelength: 522 nm).

2.7 The continues sensing property and selectivity for Cu²⁺ with TTF-PBA/Fe³⁺

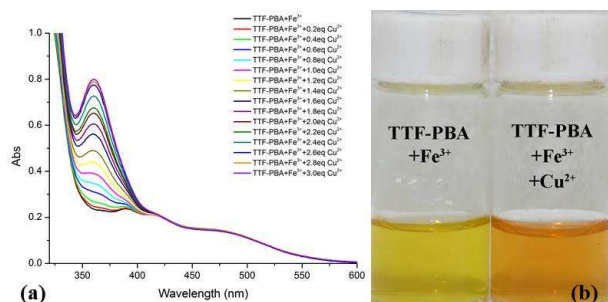


Fig. 11 (a) UV-vis spectra of TTF-PBA/Fe³⁺ in acetonitrile (2×10^{-5} mol/L) upon addition of 0.2-3.0 equiv. CuCl₂. (b) Color change of the addition 3.0 equiv. of CuCl₂ into TTF-PBA/Fe³⁺ solution (1×10^{-4} mol/L).

When Fe³⁺ was present in the solution, Cu²⁺ could also be detected sequentially by the chemosensor. As shown in Fig. 11, with the addition of 4.0 equiv. Fe³⁺, the characteristic absorption bands appeared at 389 nm, 416 nm and 482 nm. Then gradually adding Cu²⁺ into the solution, a new band at 362 nm appeared without changing of other two bands at 416 nm and 482 nm. The band at 362 nm stopped change upon addition of 3.0 equiv. Cu²⁺. With additional of 3.0 equiv. Cu²⁺, the solution color changed from orange to red. The ratio between Cu²⁺ and TTF-PBA/Fe³⁺ was proved by Job's Plot, the change happened at $[\text{Cu}^{2+}]/([\text{Cu}^{2+}] + [\text{TTF-PBA/Fe}^{3+}]) = 0.5$ (Fig. 12), which meant that Cu²⁺ and TTF-PBA/Fe³⁺ formed a complex with a ratio of 1:1. The binding constant (K_b) was estimated using Benesi-Hildebrand plot to be 2.82×10^4 L/mol (Fig. S10). The reason of the change can be explained that TTF-PBA is oxidized by Fe³⁺ at first, then the Cu²⁺ is added and in complex with the picolinamide unit of TTF-PBA. The absorption did not change obviously when other metal ions (Pb²⁺, Zn²⁺, Ni²⁺, Ag⁺, Cr³⁺, Mn²⁺, Al³⁺, Co²⁺, Pd²⁺, Hg²⁺, Fe²⁺, Cd²⁺, Ce³⁺, Bi³⁺ and Au³⁺) were added into the solution (Fig. 13).

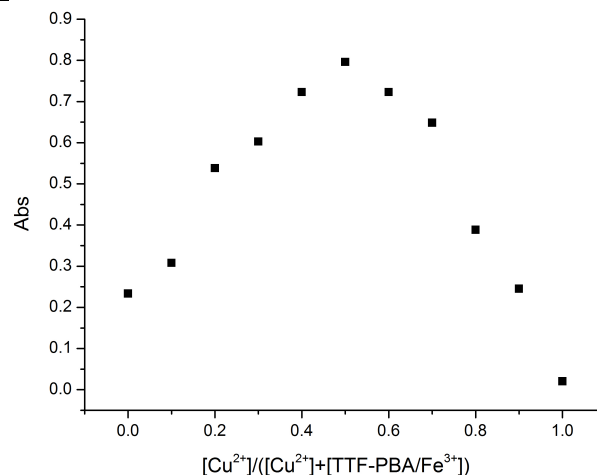


Fig. 12 Job's Plot for the complex of Cu²⁺ with TTF-PBA/Fe³⁺ determined by UV-vis spectra.

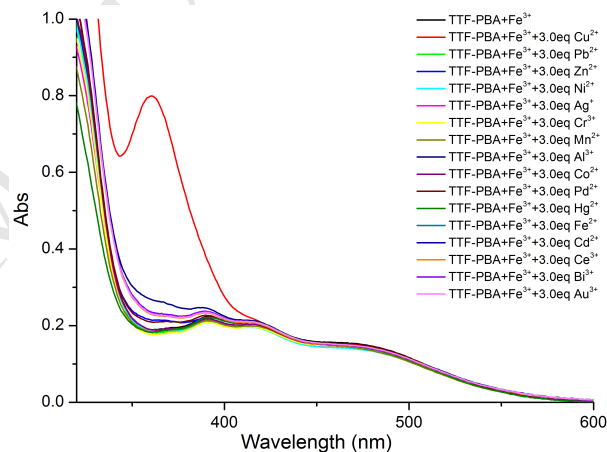


Fig. 13 UV-vis spectra of TTF-PBA/Fe³⁺ in acetonitrile (2×10^{-5} mol/L) upon addition of CuCl₂, AgNO₃, ZnCl₂, MnCl₂, NiCl₂, Hg(COOH)₂, PbCl₂, PdCl₂, CoCl₂, FeCl₂, CdCl₂, CrCl₃, AlCl₃, Ce₂(SO₄)₃, BiCl₃, AuCl₃.

3. Conclusions

In summary, a new dual chemosensor TTF-PBA for Fe³⁺ and Cu²⁺ was designed and synthesized successfully, which can be used to detect Fe³⁺ and Cu²⁺ in different signal pathways. In the new chemosensor, 2,2'-(2-iodoanthracene-9,10-diylidene)bis(4,5-bis(methylthio)-1,3-dithiole) is used as electron donor and picolinamide unit is used as electron acceptor. To elongate the π -conjugation system, phenyl group is introduced. The absorption spectrum, fluorescence spectrum and cyclic voltammograms changed upon addition of Cu²⁺ and Fe³⁺. The optical color changed within 5 seconds from yellow to orange upon the addition of Cu²⁺, and it changed to dark yellow when Fe³⁺ existed. The cyclic voltammogram of Cu²⁺/TTF-PBA changed from $E_{\text{ox}} = 0.50$ V, $E_{\text{red}} = 0.32$ V to $E_{\text{ox}} = 0.64$ V, $E_{\text{red}} = 0.80$ V (vs Ag/AgCl) upon the addition of 2.0 equiv. Cu²⁺. As for Fe³⁺/TTF-PBA, its oxidation wave disappeared, and its reduction wave appeared at $E_{\text{red}} = -0.59$ V (vs Ag/AgCl) upon the addition of 4.0 equiv. of Fe³⁺. The detection mechanism of Cu²⁺ is that Cu²⁺ complexed with picolinamide unit upon the addition of 1.0

equiv., and then the TTF unit was oxidized to cation radical (TTF^{•+}) upon the addition of more Cu²⁺. And the mechanism of Fe³⁺ detection is that Fe³⁺ oxidized the TTF unit into dication species (TTF²⁺). The fluorescence of the TTF-PBA solution was quenched in the presence of Cu²⁺ or Fe³⁺, it may be attributed to the paramagnetic nature of Cu²⁺ and Fe³⁺. The dye TTF-PBA displayed high selectivity for Cu²⁺ and Fe³⁺ over other ions including Pb²⁺, Zn²⁺, Ni²⁺, Ag⁺, Cr³⁺, Mn²⁺, Al³⁺, Co²⁺, Pd²⁺, Hg²⁺, Fe²⁺, Cd²⁺, Ce³⁺, Bi³⁺, Au³⁺, and the detection limits for Cu²⁺ and Fe³⁺ ion reached as low as 5.33×10⁻⁷ mol/L and 5.34×10⁻⁷ mol/L, respectively. Furthermore, when Fe³⁺ existed, Cu²⁺ can be detected sequentially by the sensor through the absorption spectrum and the color change observed by naked-eyes.

4. Experimental Section

4.1 Materials and measurements

All chemical reagents and solvents were purchased from commercial suppliers and were used without further purification unless otherwise noted. Triethyl phosphite was distilled before using. Dioxane was dried with metal sodium and distilled immediately prior to use. All moisture-sensitive and air-sensitive reactions were carried out under argon atmosphere.

¹H-NMR and ¹³C-NMR spectra were measured on a Bruker AM-400 spectrometer using d-chloroform as a solvent and tetramethylsilane (TMS, δ = 0 ppm) as an internal standard. The UV-vis spectra were recorded on a Varian CARY 100 spectrophotometer at room temperature. Fluorescence-emission was detected on Varian Cary Eclipse spectrophotometer at room temperature in acetonitrile. The cyclic voltammograms was obtained from CHI620e electrochemistry workstation. The supporting electrolyte was 0.1M TBAPF6 in acetonitrile. The scan rate was 100 mV•s⁻¹. The working electrode was glass carbon, the counter electrode was platinum-wire coil, and the reference electrode was Ag/AgCl.

4.2 Synthetic procedures

2-iodoanthracene-9,10-dione (**1**) and 4,5-bis(methylthio)-1,3-dithiole-2-thione (**2**) were synthesized according to literatures^{30,31}.

2,2'-(2-iodoanthracene-9,10-diylidene)-bis(4,5-bis(methylthio)-1,3-dithiole) (**3**)³²

A mixture of 2-iodoanthracene-9,10-dione (**1**) (100 mg, 0.30 mmol), 4,5-bis(methylthio)-1,3-dithiole-2-thione (**2**) (68 mg, 0.30 mmol) in toluene (10 mL) and triethyl phosphite (5 mL) was stirred at 100 °C under argon atmosphere for 1 h. Then **2** (68 mg, 0.30 mmol) was added to the reaction mixture. After the mixture was stirred overnight, the solvent were removed and the residue was purified by silica column (eluent Petroleum ether : CH₂Cl₂ = 5 : 1) to give a yellow solid in 52.51% yield, m. p. 198 - 200 °C. ¹H-NMR (400 MHz, CDCl₃) δ (ppm): 7.86 (d, J = 1.7 Hz, 1 H), 7.61 - 7.62 (dd, J₁ = 8.2 Hz, J₂ = 1.8 Hz, 1 H), 7.55 - 7.53 (m, 2 H), 7.33 - 7.30 (m, 2 H), 7.27 (d, J = 3.4 Hz, 1 H), 2.42 - 2.39 (m, 12 H).

4-bromo-N-(pyridin-2-yl)benzamide (**5**)³³

4-bromobenzaldehyde (200 mg, 1.09 mmol), pyridin-2-amine (153 mg, 1.63 mmol) and CuI (21 mg, 0.11 mmol) were mixed in 5 mL DMF. The reaction mixture was stirred at 80 °C for 24 h. Then the reactant was extracted with CH₂Cl₂ (3 × 10 mL) and washed by water (3 × 10 mL). The organic layer was dried by Na₂SO₄. After removing the solvent, the crude product was purified by silica column (eluent petroleum ether : ethyl acetate =

10 : 1) to get a white solid in 62.79% yield, m. p. 133.2 - 135.0 °C. ¹H-NMR (400 MHz, CDCl₃) δ (ppm): 8.64 (s, 1 H) 8.37 (d, J = 8.4 Hz, 1 H) 8.30 (d, J = 5.9 Hz, 1 H) 7.81 (d, J = 8.6 Hz, 2 H) 7.77 (dd, J₁ = 8.4 Hz, J₂ = 1.8 Hz, 1 H) 7.67 - 7.63(m, 2 H) 7.10 - 7.08 (m, 1 H).

N-(pyridin-2-yl)-4-(4,4,5,5-tetramethyl-1,3,2-dioxaborolan-2-yl)benzamide (**6**)³⁴

5 (200 mg, 0.72 mmol) and bis(pinacolato)diboron (367 mg, 1.44 mmol) were combined in anhydrous dioxane. Potassium acetate (213 mg, 2.16 mmol) and Pd(dppf)Cl₂ (53 mg, 0.07 mmol) were added to the mixture under argon atmosphere. The mixture was stirred at 100 °C overnight. After evaporation of the solvent, the residue was purified by silica column (eluent petroleum ether : ethyl acetate = 5 : 1) to get a brown oil in 72.03% yield. ¹H-NMR (400 MHz, CDCl₃) δ (ppm): 8.82 (s, 1 H) 8.42 (d, J = 8.4 Hz, 1 H) 8.31 (d, J = 3.6 Hz, 1 H) 7.94 (s, 4 H) 7.78 (t, J = 8.8 Hz, 1 H) 7.09 (dd, J₁ = 6.6 Hz, J₂ = 5.0 Hz, 1 H) 1.37(s, 12 H).

4-(9,10-bis(4,5-bis(methylthio)-1,3-dithiol-2-ylidene)-9,10-dihydroanthracen-2-yl)-N-(pyridin-2-yl)benzamide (TTF-PBA)

3 (168 mg, 0.24 mmol), **6** (108 mg, 0.33 mmol) and K₂CO₃ (269 mg, 1.95 mmol) were dissolved in toluene (15 mL) and water (5 mL). Then Pd(PPh₃)₄ (28 mg, 0.02 mmol) was added under Argon atmosphere. The reaction mixture was heated to reflux and stirred for 24 h. After completion of the reaction, CH₂Cl₂ (20 mL) and water (30 mL) were added into the reaction mixture. Then the organic layer was washed by water (10 mL × 3) and dried over Na₂SO₄. After the solvent was removed, the residue was purified by silica column (eluent CH₂Cl₂ : CH₃OH = 20 : 1) to get a yellow solid in 49.62% yield, m. p. 210 - 212 °C. ¹H-NMR(400 MHz, CDCl₃) δ(ppm): 8.65 (s, 1 H) 8.42 (d, J = 8.4 Hz, 1 H) 8.05 (d, J = 8.4 Hz, 2 H) 7.81 (dd, J₁ = 5.0 Hz, J₂ = 11.5 Hz, 4 H) 7.68 (d, J = 8.1 Hz, 1 H) 7.60 - 7.56 (m, 2 H), 7.34 (dd, J₁ = 3.2 Hz, J₂ = 5.6 Hz, 2 H) 7.13 - 7.05 (m, 2 H) 2.41 (s, 12 H). ¹³C-NMR(100 MHz, CDCl₃) δ(ppm): 164.21, 150.60, 146.78, 143.12, 137.57, 136.46, 134.33, 134.13, 133.43, 131.88, 130.77, 130.61, 126.98, 126.28, 125.43, 125.31, 125.01, 124.77, 124.42, 124.29, 123.96, 123.04, 122.40, 122.03, 118.93, 113.29, 28.68. ESI-MS [M + H⁺] Calcd. 761.0046 Found 761.0042.

4.3 UV-vis and fluorescence titration

TTF-PBA (7.6 mg) was dissolved in 100 mL acetonitrile to get a 1 × 10⁻⁴ mol/L solution. Then the solution was diluted to 2 × 10⁻⁵ mol/L solution. CuCl₂•2H₂O (51.0 mg) was dissolved in 10 mL acetonitrile to get 0.03 mol/L solution. A series of 3.0 mL 2 × 10⁻⁵ mol/L TTF-PBA solutions were taken in cuvettes, then 0.4 μL (0.2 equiv.), 0.8 μL (0.4 equiv.), 1.2 μL (0.6 equiv.), 1.6 μL (0.8 equiv.), 2.0 μL (1.0 equiv.), 2.4 μL (1.2 equiv.), 2.8 μL (1.4 equiv.), 3.2 μL (1.6 equiv.), 3.6 μL (1.8 equiv.), 4.0 μL (2.0 equiv.), 4.4 μL (2.2 equiv.), 4.8 μL (2.4 equiv.), 5.2 μL (2.6 equiv.), 5.6 μL (2.8 equiv.), 6.0 μL (3.0 equiv.) and 6.4 μL (3.2 equiv.) Cu²⁺ was added respectively. After mixing them for a few seconds (in 5 seconds), UV-vis and fluorescence spectra tests were taken at room temperature.

The method of Fe³⁺ titration was as the same as Cu²⁺ titration. FeCl₃ (48.7 mg) was dissolved in 10 mL acetonitrile to get 0.03 mol/L solution.

4.4 UV-vis and fluorescence for selectivity

ZnCl₂ (40.8 mg), PbCl₂ (83.4 mg), AgNO₃ (51.0 mg), NiCl₂•6H₂O (71.4 mg), CrCl₃•6H₂O (79.8 mg), MnCl₂•4H₂O (59.4 mg), FeCl₂•4H₂O (59.7 mg), Hg(COOH)₂ (95.6 mg), CdCl₂ (54.9 mg), CoCl₂•6H₂O (71.4 mg), AlCl₃ (39.9 mg), PdCl₂ (53.1

mg), $\text{Ce}_2(\text{SO}_4)_3 \cdot 4\text{H}_2\text{O}$ (121.3mg), BiCl_3 (94.6mg), AuCl_3 (123.6mg) were dissolved in 10 mL acetonitrile to get 0.03 mol/L solution respectively. Then 6.0 μL (3.0 equiv.) or 8.0 μL (4.0 equiv.) ion solution was added into 3.0 mL 2×10^{-5} mol/L TTF-PBA solution. After mixing them for a few seconds (in 5 seconds), UV-vis and fluorescence spectra tests were taken at room temperature.

4.5. Job's Plot measurements

600 μL , 540 μL , 480 μL , 420 μL , 360 μL , 300 μL , 240 μL , 180 μL , 120 μL , 60 μL and 0 μL 1×10^{-4} mol/L TTF-PBA solution were taken and transferred to cuvette. 0 μL , 0.2 μL , 0.4 μL , 0.6 μL , 0.8 μL , 1.0 μL , 1.2 μL , 1.4 μL , 1.6 μL , 1.8 μL and 2.0 μL 0.03 mol/L Cu^{2+} solution were added into each cuvette, then each cuvette was dilute to 3.0 mL. After mixing for a few seconds (in 5 seconds), fluorescence spectra tests were taken at room temperature.

4.6 Calculation of detection limit

The detection limit was determined from the fluorescence titration data based on $3\sigma/K$. Ten times of fluorescence intensity of TTF-PBA were tested and σ can be calculated. According to the result of fluorescence titrating experiment, the fluorescent intensity data of TTF-PBA were normalized between the minimum intensity and the maximum intensity respectively when excited at 430 nm. The linear regression curve was then fitted to these normalized fluorescent intensity data, and the slope K of line could be calculated.

Acknowledgements

This work is sponsored by Natural Science Foundation of Shanghai (16ZR1408000), and the National Natural Science Foundation of China (No. 21576087).

Supplementary data

$^1\text{H-NMR}$, $^{13}\text{C-NMR}$, and MS of TTF-PBA are available. Additional graphs for calculation of detection limit and binding constant can be found in ESI.

References

- Cheng, X. W.; Zhou, Y.; Fang, Y.; Rui, Q. Q.; Yao, C. *RSC Adv.*, **2015**, 5, 19465-19469.
- Fang, Y.; Ni, Y.; Choi, B.; Leo, S. Y.; Gao, J.; Ge, B.; Taylor, C.; Basile, V.; Jiang, P. *Adv. Mater.*, **2015**, 27, 3696-3704.
- Zhang, L.; Han, Y.; Zhao, F.; Shi, G.; Tian, Y.; *Anal. Chem.*, **2015**, 87, 2931-2936.
- Zhang, R. X.; Zhuang, X. Y.; Liu, S.; Song, F. G.; Liu, Z. Q. *Anal. Methods.*, **2014**, 6, 5746-5752.
- Puangploy, P.; Smanmoo, S.; Surareungchai, W.; *Sensor Actuat. B-Chem.*, **2014**, 193, 679-686.
- Zhao, X.; Tian, D.; Gao, Q.; Sun, H.; Xu, J.; Bu, X. *Dalton Trans.*, **2016**, 45, 1040-1046.
- Park, G. J.; Hwang, I. H.; Song, E. J.; Kim, H.; Kim, C. *Tetrahedron*, **2014**, 70, 2822-2828.
- Zhang, Z. M.; Shi, Y. P.; Pan, Y.; Cheng, X.; Zhang, L. L.; Chen, J. Y.; Li, M. J.; Yi, C. Q. *J. Mater. Chem. B*, **2014**, 2, 5020-5027.
- He, X.; Zhang, J.; Liu, X.; Dong, L.; Li, D.; Qiu, H.; Yin, S. *Sensor Actuat. B-Chem.*, **2014**, 192, 29-35.
- Kumar, M.; Kumar, N.; Bhalla, V.; Sharma, P. R.; Kaur, T. *Org. Lett.*, **2011**, 14, 406-409.
- Georgopoulos, P. G.; Roy, A.; Yonone Liroy, M. J.; Opiekun, R. E.; Liroy, P. J. *J. Toxicol. Env. Heal. B*, **2001**, 4, 341-394.
- Liu, X.; Zhang, N.; Bing, T.; Shangguan, D.; *Anal. Chem.*, **2014**, 4, 2289-2296.
- Wang, Y.; Wang, C.; Xue, S.; Liang, Q.; Li, Z.; Xu, S.; *Rsc Adv.*, **2016**, 6, 6540-6550.
- Yang, L.; Zhu, N. W.; Fang, M.; Zhang, Q.; Li, C. *Spectrochim. Acta, Part A*, **2013**, 109, 186-192.
- Paul, B. K.; Kar, S.; Guchhait, N. J.; *J. Photoch. Photobio. A*, **2011**, 220, 153-163.
- Fabian, J.; Nakazumi, H.; Matsuoka, M. *Chem. Rev.*, **1992**, 92, 1197-1226.
- Canevet, D.; Sallé, M.; Zhang, G. X.; Zhang, D. Q.; Zhu, D. B. *Chem. Commun.*, **2009**, 17, 2245-2269.
- Yamashita, Y.; Kobayashi, Y.; Miyashi, T. *Angew. Chem. Int. Edit.*, **1989**, 28, 1052-1053.
- Bryce, M. R.; Moore, A. J.; Hasan, M.; Ashwell, G. J.; Fraser, A. T.; Clegg, W.; Hursthouse, M. B.; Karaulov, A. I. *Chem. Int. Edit.*, **1990**, 29, 1450-1452.
- Moore, A. J.; Bryce, M. R. *J. Chem. Soc., Perkin Trans. I*, **1991**, 1, 157-168.
- Lerouge, M. H.; Chesneau, B.; Allain, M.; Hudhomme, P.; *J. Org. Chem.*, **2012**, 77, 2441-2445.
- Ma, Y.; Lai, G.; Li, Z.; Wang, C.; Shen, Y. *Tetrahedron*, **2015**, 71, 8717-8724.
- Mandal, S. K.; Que, L.; *Inorg. Chem.*, **1997**, 36, 5424-5425.
- Ding, H.; Liang, C. S.; Sun, K. B.; Wang, H. J.; Hiltunen, K.; Chen, Z. J.; Shen, J. C. *Biosens. Bioelectron*, **2014**, 59, 216-220.
- Gillissen, M. A. J.; Voets, I. K.; Meijer, E. W.; Palmans, A. R. A. *Polym. Chem.*, **2012**, 3, 3166-3174.
- Chen, G.; Bouzan, S.; Zhao, Y. M. *Tetrahedron Lett.*, **2010**, 51, 6552-6556.
- Gong, Z.; Zhong, Y.; *Organometallics*, **2013**, 32, 7495-7502.
- Guldi, D. M.; Sánchez, L.; Martin, N.; *J. Phys. Chem. B*, **2012**, 105, 7139-7144.
- Huang, R.; Zuo, H.; Zhang, L.; Wang, C.; Shen, Y. *Polym. Bull.*, **2015**, 72, 2527-2536.
- Choi, W.; Harada, D.; Oyaizu, K.; Nishide, H. *J. Am. Chem. Soc.*, **2011**, 133, 19839-19843.
- Hasegawa, M.; Takeda, K.; Kuwatam, Y.; Yoshida, M.; Matsuyama, Iyoda, H. M. *J. Sulfur. Chem.*, **2009**, 30, 301-308.
- Chen, G.; Bouzan, S.; Zhao, Y. M.; *Tetrahedron Lett.*, **2010**, 51, 6552-6556.
- Yang, S. Z.; Yan, H.; Ren, X. Y.; Shi, X. K.; Li, J.; Wang, Y. L.; Huang, G. S. *Tetrahedron*, **2013**, 69, 6431-6435.
- Ma, Y.; Leng, T.; Lai, G.; Li, Z.; Xu, X.; Zou, J.; Shen, Y.; Wang, C. *Tetrahedron*, **2016**, 72, 2219-2225.